LINEAR AND NONLINEAR SOURCES OF SUB-CONVECTIVE PRESSURE FLUCTUATIONS USING KRAICHNAN'S APPROACH

Bhavika Sharma, Shishir Damani, Gerrit Vander Wiel, Eric Totten, William J. Devenport, Todd K. Lowe
Kevin T. Crofton Department of Aerospace and Ocean Engineering
Virginia Polytechnic Institute and State University
Blacksburg, VA 24061
bhavika@vt.edu

ABSTRACT

This study investigates sub-convective wall-pressure source mechanisms using Kraichnan's formulation of the pressure Poisson equation. Using synchronized wall-pressure and wall-parallel stereoscopic PIV measurements in a smooth-wall turbulent boundary layer at $M = 0.066$ and $x_2/\delta = 0.26$, pressure–velocity cross-spectral analysis is used to quantify linear and nonlinear source contributions in the wavenumber–frequency domain. Beyond separating linear and nonlinear mechanisms, the framework resolves the relative contributions of constituent nonlinear source terms. Results show that nonlinear contributions remain comparable to mean-shear-related sources and become increasingly important outside the low-wavenumber, low-frequency regime, indicating a scale-dependent partitioning of pressure-generating mechanisms.

INTRODUCTION

The identification of sub-convective wall-pressure fluctuations has remained challenging due to their weak spectral footprint and experimental limitations, despite their importance to cabin noise and structural vibration (Damani *et al.*, 2022). Recent advances in spatially averaging pressure sensing have enabled experimentally resolved measurements of the full wavenumber–frequency wall-pressure spectrum, overcoming long-standing spatial aliasing limitations that obscured the sub-convective regime. These novel measurements revealed sub-convective pressure levels and spectral trends in close agreement with classical Chase-model predictions, providing an experimental capability that had not previously been demonstrated (Damani *et al.*, 2025).

Turbulent boundary layers contain large-scale coherent motions, including large-scale motions (LSMs) and very-large-scale motions (VLSMs), whose signatures have been extensively characterized in both experiments and simulations (Sharma *et al.*, 2025; Lee & Sung, 2011). These motions have motivated growing interest in understanding how turbulent structures contribute to wall-pressure generation, particularly through pressure–velocity correlations (Naka *et al.*, 2015; Anantharamu & Mahesh, 2020; Butt *et al.*, 2024).

The relationship between turbulent velocity fluctuations and wall pressure has classically been described using source formulations based on the pressure–Poisson equation, Eq. (1), following the developments of Kraichnan (1956*a*) and Ffowcs Williams (1965). In particular, Chang *et al.* (1999) showed that wall-pressure generation arises from multiple source mechanisms involving both mean-shear-related (linear) and turbulence-interaction (nonlinear) contributions, whose relative importance varies with wall-normal position. More recently, Anantharamu & Mahesh (2020) demonstrated that pressure-generating sources are strongly scale dependent, with buffer-layer sources dominating the classical spectral peak and broader distributed sources contributing at lower frequencies. More recent experimental studies have advanced the pressure–velocity correlation picture by showing that wall-pressure signals contain substantial information about large-scale turbulent motions.Dacome et al. (Dacome *et al.*, 2025) showed that pressure–velocity correlations scale coherently with logarithmic-region large-scale structures, while Deshpande et al. (Deshpande *et al.*, 2025) linked outer-scaled wall-pressure sources to energetic large-scale motions, underscoring the importance of resolving coherent pressure structures across scales.

Motivated by these developments, experimental quantification of the relative linear and nonlinear source contributions to sub-convective pressure fluctuations remains limited, particularly using synchronous pressure–velocity measurements. The present study addresses this gap through Kraichnan's approach to pressure–Poisson framework using simultaneous wall-pressure and wall-parallel stereoscopic PIV measurements at a representative wall-normal location in a smooth-wall turbulent boundary layer. By evaluating pressure–velocity source terms in the wavenumber–frequency domain, this work provides a step towards resolving the flow physics underlying sub-convective pressure generation.

Extension of the Kraichnan's Framework

The Pressure-Poisson equation (PPE) for wall pressure is an exact rearrangement of the incompressible Navier-Stokes. Solving for the fluctuating wall pressure of a two-dimensional flow yields the following:

$$p'(x,t) = \frac{\rho_0}{2\pi} \int_V \frac{1}{r} \left[2\frac{\partial U_1}{\partial y_2}\frac{\partial u_2}{\partial y_1} + \frac{\partial^2 (u_i u_j - \overline{u_i u_j})}{\partial y_i \partial y_j} \right]_{(y,t)} dV(y) \quad (1)$$

where the term $\frac{\partial U_1}{\partial y_2}\frac{\partial u_2}{\partial y_1}$, and $\frac{\partial^2 (u_i u_j - \overline{u_i u_j})}{\partial y_i \partial y_j}$ are often referred to as the mean shear (MS) and turbulence-turbulence (TT) terms respectively and each term definition is as described in Blake (2017).

Kraichnan (1956*b*) and Blake (2017) showed that in a boundary layer where flow in the (x_1, x_3) directions is homogeneous, the MS and TT terms of Eq. (1) reduce to a single integral form with algebraic expressions of velocity terms and the wall normal velocity gradient in wavenumber—frequency space.

$$\tilde{p}(k_1,k_3,\omega) = \frac{\rho_0}{k_{13}} \int_0^{R_\infty} e^{-k_{13}y_2} \Big(2ik_i\tilde{u}_2 \frac{\partial U_i}{\partial y_2} - k_ik_j\widetilde{u_iu_j} + 2ik_ik_{13}\widetilde{u_iu_2} + k_{13}^2\widetilde{u_2u_2}\Big) dy_2 \quad (2)$$

Equation (2) expresses wall-pressure fluctuations as a wall-normal integral of velocity sources, providing the general source framework used in this study. Here, the left-hand side represents the Fourier transform of the wall pressure, while the right-hand side contains the integrated contributions of distinct velocity source terms across the boundary layer. In this formulation, $k_{13} = \sqrt{k_1^2 + k_3^2}$ is the magnitude of the wall-parallel wavenumber vector, U_i denotes the mean velocity component, $\tilde{u}_2$ is the Fourier transform of the wall-normal velocity fluctuation, and $\widetilde{u_iu_j}$ represents the transformed Reynolds-stress terms. The exponential weighting $e^{-k_{13}y_2}$ accounts for the wall-normal dependence of these source contributions (Glegg & Devenport, 2023).

$$\Phi_{pp}(k_1,k_3,\omega) = \frac{\rho_0}{k_{13}} \int_0^{R_\infty} e^{k_{13}y_2} \Big(2ik_i\Phi_{p2} \frac{\partial U_i}{\partial y_2} - k_ik_j\Phi_{pij} + 2ik_ik_{13}\Phi_{pi2} + k_{13}^2\Phi_{p22}\Big) dy_2 \quad (3)$$

Correlating Eq. (2) with the wall-pressure field and taking the ensemble average yields Eq. (3), which relates the wall-pressure spectrum to pressure–velocity and pressure–velocity–product cross-spectral source terms while preserving the linear integral structure. In this form, the wall-pressure spectrum is expressed as a weighted sum of distinct source contributions, enabling the relative importance of the individual terms in the integrand to be examined experimentally.

For a given wall-parallel measurement plane, each source term can be directly compared to assess its contribution to the measured pressure spectrum. For finite-sized sensors, an area-averaged form of Eq. (3) preserves the same structure, with each term weighted by the sensor area-sensitivity function. The Kraichnan-based framework used here follows a related formulation previously employed by the authors for rough-wall turbulence in Sharma *et al.* (2026), and is applied in the present smooth-wall study to examine linear and nonlinear source contributions, while further resolving the relative contributions of the individual source terms to sub-convective pressure fluctuations. Evaluating the formulation at zero spanwise wavenumber ($k_3 = 0$), corresponding to the component captured by the streamwise pressure array. To conform with the coordinate system used here, the formulation is rewritten with the wall-normal coordinate represented by x_2, and the source terms are adjusted accordingly. Table 1 defines the individual source terms appearing on the right-hand side of Eq. (3), where dx_2 is taken as the 1 mm laser-sheet thickness.

EXPERIMENTAL SETUP
Stability Wind Tunnel

The experimental campaign was conducted in the Virginia Tech Stability Wind Tunnel (VTSWT), a closed-circuit, single-return subsonic facility. Details of the facility and smooth-wall test conditions are given in Sharma *et al.* (2025); Damani *et al.* (2022). Figure 1 shows the smooth-wall boundary-layer development at $M = 0.066$ under nominal zero-pressure-gradient conditions. The mean boundary-layer profile was characterized using a Vectoflow GmbH boundary-layer rake positioned at $x = 2.68$ m downstream of the tunnel origin, from which the smooth-wall reference profile and associated boundary-layer parameters were obtained.

Table 1: Kraichnan source terms appearing in Eq. 3 and their physical interpretation.

Term	Expression	Description
(A)	$2\rho_0 ik_1 e^{-k_1x_2} \frac{\partial U_1}{\partial x_2} \Phi_{u_2,p}\, dx_2$	Mean shear
(B)	$\rho_0 k_1^2 e^{-k_1x_2} \Phi_{u_1u_1,p}\, dx_2$	Reynolds stress
(C)	$2\rho_0 ik_1^2 e^{-k_1x_2} \Phi_{u_1u_2,p}\, dx_2$	Transport
(D)	$\rho_0 k_1^2 e^{-k_1x_2} \Phi_{u_2u_2,p}\, dx_2$	Wall-normal energy

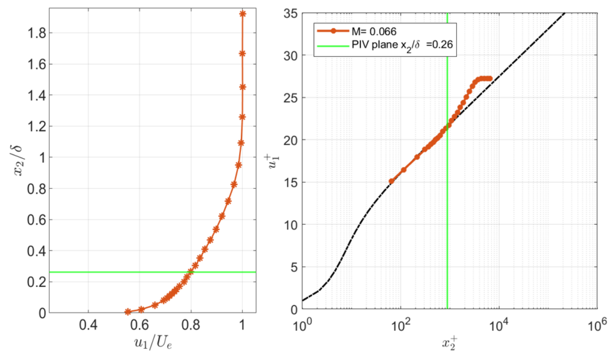

Figure 1: Smooth-wall boundary-layer profiles at $x_1 = 2.68$ m for $M = 0.066$, with comparison against the Spalding profile shown on the right.

Stereoscopic Wall Parallel PIV

To investigate near-wall turbulent motions, a wall-parallel (x_1, x_3) stereoscopic PIV system with a traversing camera–laser arrangement was employed. Time-resolved 2D3C velocity fields were acquired 2.45 m downstream of the tunnel origin using four Phantom v2512 cameras, configured to capture two overlapping stereo regions and combined into a field of view of 518 mm (streamwise) by 178 mm (spanwise). Cameras were arranged at off-axis angles of 38° and 40° to provide the stereoscopic geometry, following the configuration of Sharma *et al.* (2026), with modifications to enable traversing measurements at multiple wall-normal locations. Data were acquired at 5 kHz for 4.8 s per run and processed in DaVis 10.2 using a multi-pass cross-correlation scheme (64×64 px initial window followed by 32×32 px refinement at 75% overlap), yielding a final vector spacing of 2.25 mm. Each run captured 24000 snapshots and statistics for 4 such runs are considered in the analysis below.

Sub-convective Pressure Sensing Array

Fluctuating wall-pressure measurements were obtained using a flush-mounted linear array of 90 area-averaging sensors embedded in a smooth-wall panel as described in Van-

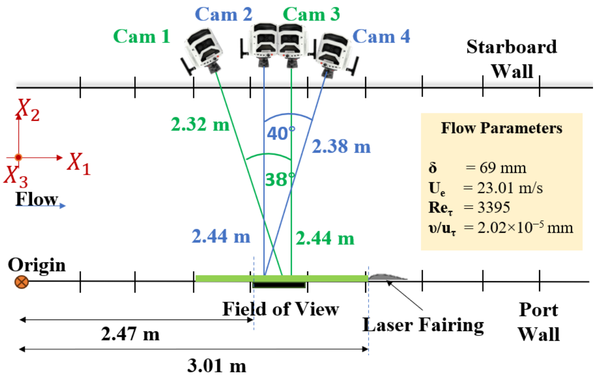

Figure 2: (a) Schematic of the experimental setup showcasing wall parallel PIV and pressure sensing array placement inside the test-section s of the Virginia Tech Stability Wind Tunnel.

der Wiel *et al.* (2026). Each sensor consists of a quarter-inch G.R.A.S. 40PH-10 microphone, selected for its wide dynamic range to resolve low-energy sub-convective pressure fluctuations. The microphones are mounted beneath a porous surface consisting of tiny pores connected to a cavity, enabling spatial averaging of pressure over the sensing area and reducing spatial aliasing, particularly in the sub-convective region.

Each individual sensor on the array is oriented with its longest dimension in the spanwise direction, and the sensors are stacked tightly in the streamwise direction. This enables spanwise averaging of the wall pressure field, effectively measuring the $\Phi_{pp}(k_1, k_3 = 0, \omega)$ component of the wall-pressure spectrum. The streamwise sensor-to-sensor spacing is 5.5 mm and has the properties as described in Vander Wiel *et al.* (2026).

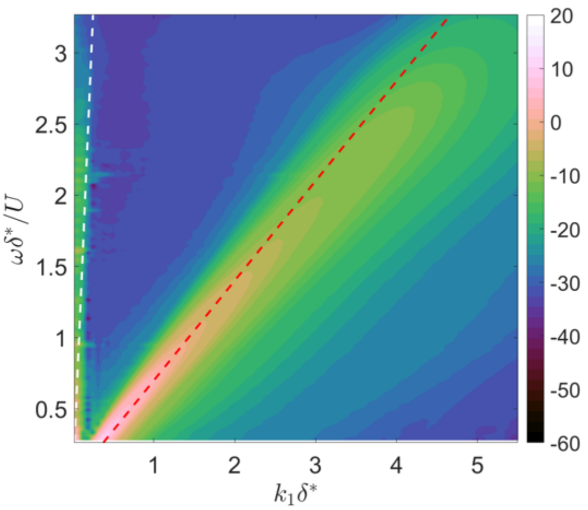

Figure 3: (a) Normalized wavenumber–frequency spectrum of wall-pressure fluctuations at $M = 0.066$.

RESULTS

Experiments were conducted in a smooth-wall turbulent boundary layer with edge velocity $U_e = 23.01$ m/s, boundary-layer thickness $\delta = 69$ mm, and friction Reynolds number $Re_\tau = 3395$. The wall-parallel PIV measurement plane was positioned at $x_2/\delta = 0.26$ and lies in the outer-layer region, which is associated with large-scale turbulent motions.

Wall Pressure Spectrum

Figure 3 displays the wall-pressure wavenumber–frequency spectrum measured by the sub-convective pressure sensing array described above. Here, the red dashed line represents the mean convective line and the white dashed line represents the acoustic line. The frequency has been scaled using the boundary layer displacement thickness and the edge velocity, $\omega\delta^*/U_e$, the wavenumber has been normalized using the displacement thickness, $k_1\delta^*$, and the spectral levels have been scaled using the mixed scaling ($\Phi_{pp}U_e/\tau_w^2\delta^{*2}$). We observe an asymmetric and compact convective ridge (about the red dashed line) with a much steeper roll-off in the sub-convective regime (between the two dashed lines) than in the super-convective regime (right of the red dashed line). The convective ridge displays a small dependency on frequency, wherein the true convective velocity, (U_c), is decreasing as the frequency is increased. This is representative of the hierarchy of coherent motions in canonical smooth wall turbulent boundary layer flow. The difference in levels between those seen along the convective line and those seen in the sub-convective regime is between 25 and 35 dB, with this difference growing as the frequency is increased.

Coherence in Physical Space

As a precursor to the wavenumber–frequency source-term analysis, the coherence between wall pressure and the source-related quantities is first examined. Figure 4 shows contours of $10\log_{10}(\gamma^2)$ as a function of streamwise separation, Δx_1, and frequency, f, where lighter contours indicate stronger pressure-coupled coherence. The frequency axis identifies the temporal scales over which each source-related quantity remains correlated with wall pressure, while the separation axis reflects the streamwise extent of that correlated structure. Together, these maps provide a measure of how strongly and over what spatial and temporal scales each source term is coupled to the measured pressure field.

The coherence maps show organized pressure-coupled signatures for all source-related quantities, with the strongest coherence observed for *pv*, followed by *puu*, *puv*, and *pvv*. The coherence is concentrated primarily in the low-frequency regime, indicating that the largest pressure-coupled structures contribute most strongly to the measured correlations. For the present analysis, the total number of snapshots is $N = 96{,}000$ with $N_{rec} \approx 1500$, giving a minimum significant coherence level of approximately -22 dB; coherence levels above this threshold are therefore interpreted as statistically meaningful.

These correlations provide the physical basis for the subsequent decomposition. Frequency-dependent cross-spectral relationships are first formed from the pressure–source data and then Fourier transformed in streamwise separation, Δx_1, to obtain the corresponding wavenumber–frequency spectra. The comparatively weaker coherence associated with terms involving wall-normal velocity should, however, be interpreted with care. Because the measurements rely on wall-parallel stereoscopic PIV, larger uncertainty is expected in the wall-normal velocity component, which may influence the inferred coherence levels for terms such as *puv* and *pvv*. Lower coherence in these terms, therefore, does not necessarily imply diminished physical importance, but rather motivates interpreting their contributions together with the associated uncertainty in the source-term analysis that follows.

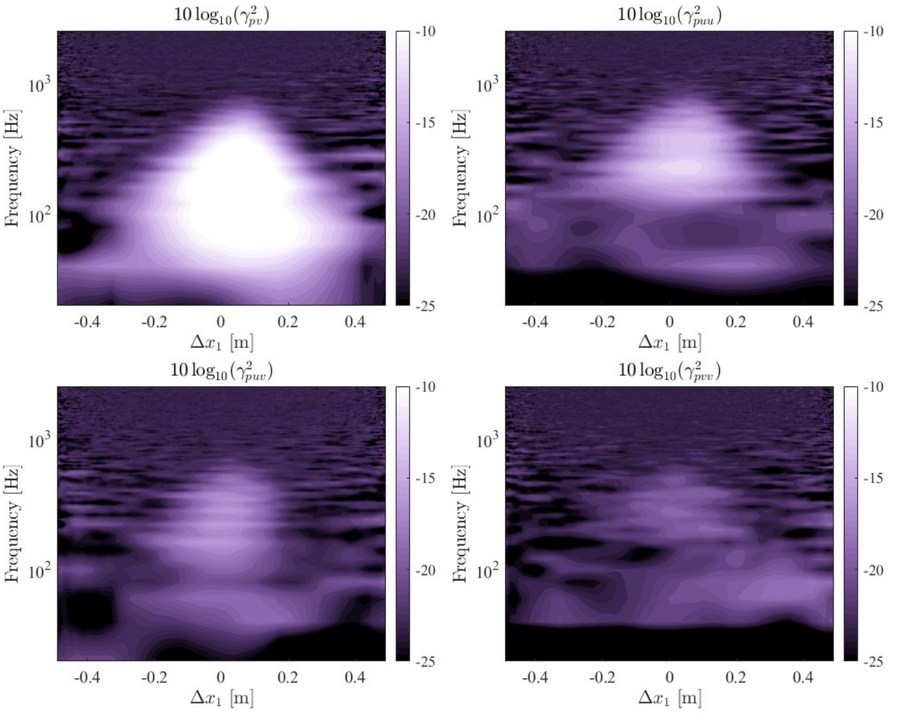

Figure 4: Magnitude-squared coherence, $10\log_{10}(\gamma^2)$, between wall pressure and the source-related quantities *pv*, *puu*, *puv*, and *pvv* as functions of Δx_1 and f. Minimum significant coherence is -22 dB.

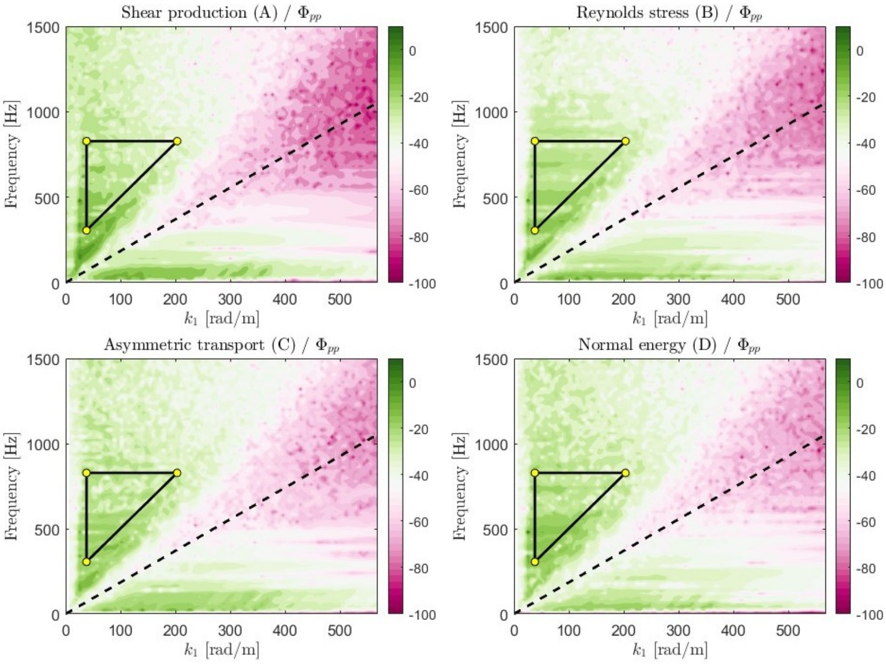

Figure 5: Wavenumber–frequency magnitude spectra (real-valued) of the ratio between correlated wall pressure and the Kraichnan source terms defined in Table 1 for the smooth-wall boundary layer. The black dashed line indicates the convective scaling relation $f = 0.7U_e k_1/2\pi$.

Source Terms Spectra

Figure 5 presents the normalized real-valued contributions of the source terms defined in Table 1 at $x_2/\delta \approx 0.26$. The contours show the real part of each source-term ratio relative to the measured wall-pressure spectrum, Φ_{pp}, expressed on a dB scale in the $(k_1, k_3 = 0, f)$ domain. Because Φ_{pp} is a real-valued quantity, only the real component of the correlated source terms is considered here, representing the physically contributing portion of each term. Contour levels approaching 0 dB indicate source contributions locally comparable in magnitude to the wall-pressure spectrum, whereas increasingly negative levels indicate weaker relative contributions. Each contour is similar to Figure 3, with the black dashed line coinciding with the red dashed line depicting the convective ridge. The sub-convective regime is to the left of the black dashed line. A triangular region is selected (marked in black) to facilitate comparison within the low-wavenumber, low-frequency portion of the spectrum associated with sub-convective pressure fluctuations.

Within the triangular region, the averaged contributions are -19.58 dB (A), -20.74 dB (B), -20.65 dB (C), and -19.40 dB (D), with corresponding median uncertainties of 0.24 dB, 0.11 dB, 0.39 dB, and 0.28 dB, respectively. Uncertainties in the wavenumber–frequency spectrum were evaluated by propagating the uncertainties in the cross-spectral density function (Sharma *et al.*, 2026). These values indicate that the mean-shear-related (A) and wall-normal energy (D) terms provide slightly stronger contributions, while the transport-related term (C) is marginally weaker, and the Reynolds stress divergence term (B) remains the smallest.

To further examine the relative contributions of the source terms, slices of the wavenumber–frequency spectrum are considered at fixed frequencies and wavenumbers. At low frequency (e.g., $f = 200$ Hz), the mean-shear-related term (A) exhibits the largest contribution across the range of wavenumbers, with term D following closely and terms C and B progressively weaker. This indicates that, at large temporal scales, pressure fluctuations are primarily influenced by mean-shear mechanisms. At higher frequencies (e.g., $f = 1000$ Hz), however, the separation between the terms diminishes significantly, with all contributions approaching similar magnitudes, suggesting a more distributed source balance at smaller temporal scales.

A similar trend is observed in slices at a fixed wavenumber. At low wavenumber ($k_1 = 50$ rad/m), corresponding to large spatial scales, term A slightly dominates at low frequencies, but this dominance weakens with increasing frequency as nonlinear contributions become comparable. At higher wavenumbers ($k_1 = 200$ rad/m), the distinction between linear and nonlinear terms is further reduced, and all contributions remain of similar magnitude across the frequency range.

Taken together, these slices indicate that mean-shear-related contributions are strongest in relatively low-wavenumber, low-frequency portion of the spectrum, while the relative distinction between linear and nonlinear contributions diminishes at higher wavenumbers and frequencies. This behavior is consistent with the observations of Chang *et al.* (1999), who showed that mean-shear and turbulence–turbulence source contributions remain of comparable magnitude and that their relative importance varies with spectral scale. In this context, the present results suggest that, even at a single wall-normal plane, nonlinear terms do not act merely as secondary corrections to the mean-shear contribution, but remain comparable contributors over significant portions of the spectrum.

A similar coexistence of linear and nonlinear source contributions is also observed in rough-wall turbulent boundary layers (Sharma *et al.*, 2026). At comparable $x_2/\delta = 0.255$, rough-wall measurements indicate that pressure fluctuations arise from a combination of both linear and nonlinear source mechanisms, although roughness modifies their relative weighting. In this sense, both smooth- and rough-wall cases suggest that sub-convective pressure generation is not governed by a single dominant mechanism, but reflects a wall-normal and scale-dependent balance of source contributions.

The concentration of elevated contributions at relatively low k_1 and low f is further consistent with large-scale coherent motions, including superstructures characterized by long streamwise extent and slow temporal evolution. Although the present analysis does not uniquely identify these structures, the observed trends are consistent with prior studies that have associated low-frequency wall-pressure fluctuations with large-scale turbulent motions Gibeau & Ghaemi (2021); Butt *et al.* (2024); Deshpande *et al.* (2025). The results therefore suggest that such large-scale motions may be linked to strong mean-shear-driven pressure generation, while at smaller spatial and temporal scales, asymmetric transport- and wall-normal-energy-related mechanisms become increasingly important. Further analysis is needed to establish these connections more definitively.

Conclusions

An experimental implementation of Kraichnan's source decomposition has been used to examine source-term contributions to sub-convective wall-pressure fluctuations in a smooth-wall turbulent boundary layer using synchronized wall-pressure and wall-parallel PIV measurements at $M = 0.066$ and $x_2/\delta = 0.26$. The principal findings are summarized as follows:

1. Pressure–velocity coherence exhibits organized coupling for all source-related quantities, strongest for *pv* and progressively weaker for *puu*, *puv*, and *pvv*, with coherence concentrated in the low-frequency sub-convective regime.
2. Sub-convective wall-pressure fluctuations arise from both linear mean-shear and nonlinear turbulence-interaction mechanisms, demonstrating that pressure generation in this regime is not governed solely by linear processes.
3. Beyond distinguishing linear and nonlinear contributions, the present framework resolves the relative contributions of the constituent nonlinear source terms, showing that transport- and wall-normal-energy-related mechanisms contribute comparably to pressure generation and participate in a scale-dependent redistribution of source strength.
4. The relative importance of these mechanisms depends on spectral scale: mean-shear-related contributions dominate the low-wavenumber, low-frequency sub-convective regime, while smaller scales exhibit a more distributed balance among coupled source processes.

Overall, the results provide an experimental framework for examining source mechanisms underlying sub-convective wall-pressure fluctuations and a basis for extending this analysis across additional wall-normal locations and more complex turbulent boundary layers.

ACKNOWLEDGEMENTS

The authors would like to thank the Office of Naval Research, and in particular Dr. Yin Lu Young, for their support of this work under grants N00014-22-1-2789, N00014-24-1-2344 and N00014-26-1-2106.

REFERENCES

Anantharamu, S. & Mahesh, K. 2020 Analysis of wall-pressure fluctuation sources from direct numerical simulation of turbulent channel flow. *Journal of Fluid Mechanics* **898**, A17.

Blake, William K. 2017 *Mechanics of Flow-Induced Sound and Vibration*, 2nd edn., , vol. 2. London: Academic Press.

Butt, Humza, Damani, Shishir, Devenport, William J & Lowe, Todd 2024 Identification of sources of sub-convective wall pressure fluctuations using space-time pressure-velocity correlations. In *30th AIAA/CEAS Aeroacoustics Conference (2024)*, p. 3166.

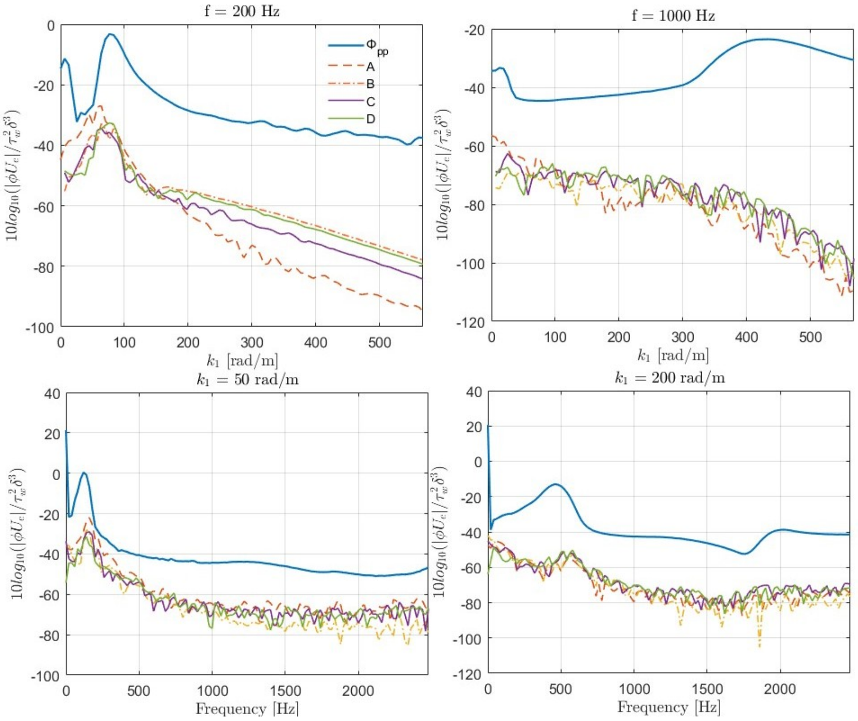

Figure 6: Normalized Kraichnan source contributions slices at frequency (top) and wavenumber(bottom)at $y/\delta \approx 0.26$, showing real-valued ratios relative

Chang, P. A., Piomelli, U. & Blake, W. K. 1999 Relationship between wall pressure and velocity-field sources. *Physics of Fluids* **11** (11), 3434–3448.

Dacome, Giulio, Lazzarini, Lorenzo, Talamelli, Alessandro, Bellani, Gabriele & Baars, Woutijn J. 2025 Scaling of wall-pressure–velocity correlations in high-reynolds-number turbulent pipe flow. *Journal of Fluid Mechanics* **1013**, A48.

Damani, S., Butt, H., Banks, J. T., Srivastava, S., Balantrapu, N. A., Lowe, T. & Devenport, W. J. 2022 Low-wavenumber wall pressure measurements in zero-pressure gradient boundary layer flow.

Damani, Shishir, Butt, Humza, Totten, Eric, Devenport, William John & Lowe, Todd 2025 Measurement and analysis of sub-convective wall pressure fluctuations in turbulent boundary layer flows. *Journal of Fluid Mechanics* **1014**, A26.

Deshpande, Rahul, Hassanein, Abdelrahman & Baars, Woutijn J. 2025 Source locations and convection velocities of outer-scaled wall-pressure fluctuations in canonical turbulent boundary layers. *arXiv preprint arXiv:2508.19940* .

Ffowcs Williams, J. E. 1965 Surface pressure fluctuations induced by boundary-layer flow at finite mach number. *Journal of Fluid Mechanics* **22** (3), 507–519.

Gibeau, Bradley & Ghaemi, Sina 2021 Low-and mid-frequency wall-pressure sources in a turbulent boundary layer. *Journal of Fluid Mechanics* **918**, A18.

Glegg, Stewart A. L. & Devenport, William J. 2023 *Aeroacoustics of Low Mach Number Flows: Fundamentals, Analysis, and Measurement*, 2nd edn. Academic Press.

Kraichnan, R. H. 1956*a* Pressure fluctuations in turbulent flow over a flat plate. *Journal of the Acoustical Society of America* **28** (3), 378–390.

Kraichnan, Robert H. 1956*b* Pressure fluctuations in turbulent flow over a flat plate. *The Journal of the Acoustical Society of America* **28** (3), 378–390.

Lee, Jae Hwa & Sung, Hyung Jin 2011 Very-large-scale motions in a turbulent boundary layer. *Journal of Fluid Mechanics* **673**, 80–120.

Naka, Y., Stanislas, M., Foucaut, J.-M., Coudert, S., Laval, J.-P. & Obi, S. 2015 Space–time pressure–velocity correlations in a turbulent boundary layer. *Journal of Fluid Mechanics* **771**, 624–675.

Sharma, Bhavika, Damani, Shishir, Vander Wiel, Gerrit, Totten, Eric, Hales, Alistair D. G., Devenport, William J. & Lowe, Todd 2026 Dynamic footprints of sub-convective pressure sources in rough-wall turbulence. In *AIAA/CEAS Aeroacoustics Conference*. Proceedings.

Sharma, Bhavika, Hales, Alistair, Butt, Humza, Damani, Shishir, Totten, Eric D, Devenport, William J, Lowe, Todd & Colbrook, Matthew 2025 Characterizing superstructures in rough-wall turbulence. In *AIAA AVIATION FORUM AND ASCEND 2025*, p. 3493.

Vander Wiel, Gerrit, Totten, Eric, Damani, Shishir, Hales, Alistair, Sharma, Bhavika, Devenport, William J. & Lowe, Todd 2026 Scaling of sub-convective wall pressure fluctuations in a turbulent boundary layer. In *AIAA/CES Aeroacoustics Conference*.